Excited State Deactivation of Indan-1-ylidene and Fluoren-9-ylidene Malononitrile‡

Leandro A. Estrada, Antonio Francés-Monerris, Igor Schapiro, Massimo Olivucci and Daniel Roca-Sanjuán

DOI: 10.1039/b000000x

Table of Contents

1. General

Commercially available reagents were used as received from the chemical suppliers unless otherwise noted. Reactions that required anhydrous conditions were carried out under an inert atmosphere of argon in flame-dried glassware. Toluene, and THF were dried using a Solvent Purification System. Pyridine and DMF were dried overnight over $MgSO_4$, stirred for 2 hours over CaH_2 and then distilled under reduced pressure prior to use (T=66–69 ºC/P=70 torr and T=60–62 ºC/P=30 torr for pyridine and DMF respectively). All reactions were monitored using F250 silica gel 60 M analytical TLC plates with UV detection (λ = 254 and 365 nm). Hanessian solution and iodine vapors were also used as developing agents depending on the nature of the material. Silica gel (60Å, 40–63 µm) was used as stationary phase for column chromatography.

Melting points (uncorrected) were measured by using a capillary melting point apparatus. FT–Infrared was recorded using neat samples. NMR experiments were acquired with working frequencies of 300.0 MHz for ^{1}H, and 75.5 MHz for ^{13}C experiments. The shifts were reported in parts per million (ppm) and referenced to the residual resonance signal of commercially available CDCl3 (δ = 7.26 ppm). Low resolution mass spectra were recorded on a quadrupole mass analyzer instrument equipped with a direct insertion probe (ionisation 70 eV), and coupled to a gas chromatograph. MALDI–TOF MS were recorded using dithranol as matrix for compound ionisation when measurements of neat compounds were unsatisfactory.

2. Synthetic procedures and characterisation

The utilised synthetic procedure for Knoevenagel condensation of the commercially available aromatic ketones with malononitrile is a slight variation of that previously published by our group.[1]

Indan-1-ylidene malononitrile (IM). Commercially available 1-indanone (330 mg, 2.5 mmol), and malononitrile (1.65 g, 25 mmol) were suspended in 5 mL of anhydrous pyridine under Argon atmosphere. The brown solution was then heated to 80 ºC for 1 hour, whereby experienced a change of color to purple. After addition of 10 mL of EtOH, the mixture was allowed to cool to room temperature and then further to –20 ºC for 2 hours. The formed crystals were then filtered, washed with chilled EtOH (3x10 mL) and then pentane. Gray color needles were obtained (328 mg, 73% yield). This compound has been reported previously.[2] Characterisation data agreed accordingly (mp, ^{1}H NMR, ^{13}C NMR) mp 154–158 ºC (lit.157–159 ºC). IR (neat, cm^{-1}) 2228, 1564. ^{1}H NMR ($CDCl_3$, 300 MHz) δ (ppm) 8.37–8.42 (d, *J*=8.1 Hz, 1H), 7.56–7.65 (t, *J*=7.2 Hz, 1H), 7.40–7.51 (m, 2H), 3.26–3.31 (m, 2H), 3.17–3.23 (m, 2H). ^{13}C NMR ($CDCl_3$, 75.5 MHz) δ (ppm) 29.6, 34.6, 74.4, 112.9, 113.5, 126.1, 126.2, 128.1, 135.1, 135.6, 154.1, 179.2. GC–MS(EI): m/z 132.2 [$M^{\cdot+}$]. Calcd for [C_9H_8O] 132.15.

Fluoren-9-ylidene malononitrile (FM). Commercially available 9-fluorenone (450 mg, 2.5 mmol), and malononitrile (1.65 g, 25 mmol) were suspended in 5 mL of anhydrous pyridine under Argon atmosphere. The brown solution was then heated to 80 ºC for 1 hour, whereby experienced a change of color to red. After addition of 10 mL of EtOH, the mixture was allowed to cool to room temperature and then further to –20 ºC for 2 hours. The formed precipitate was then filtered, washed with chilled EtOH (3x10 mL) and then pentane. Recrystallisation followed from $CHCl_3$. Red colored needles were obtained (483 mg, 84% yield). This compound has been reported previously.[3] Characterisation data agreed accordingly, except those from ^{13}C NMR.[4] (mp, FTIR, ^{1}H NMR) mp 226–228 ºC (lit.237–238 ºC). IR (neat, cm^{-1}) 2230, 1570. ^{1}H NMR ($CDCl_3$, 300 MHz) δ (ppm) 8.32–8.38 (d, *J*=7.8 Hz, 2H), 7.46–7.58 (m, 4H), 7.28–7.45 (td, J_1=1.5 Hz, J_2=7.5 Hz, 2H). ^{13}C NMR ($CDCl_3$, 75.5 MHz) δ (ppm) 75.9, 113.3, 120.7, 126.9, 129.2, 134.2, 134.7, 143.3, 161.6. GC–MS(EI): m/z 228.4 [$M^{\cdot+}$]. Calcd for [$C_{16}H_8O$] 228.64.

3. Steady state UV-Vis absorption measurements

Absorption spectra were recorded using a double-beam spectrophotometer, accurate to ± 0.3 nm. The solution concentration of the compounds was at approximately 1.0 μM in spectroscopic grade solvents for first absorbance measurements. For molar absorption coefficient calculations in toluene, after calculation of extinction coefficient from the first taken absorbance, five solutions of variable concentration were prepared for optical densities ranging within linear regime. The molar decadic absorption coefficient (ε) was calculated by plotting five absorbance values versus the corresponding concentrations of the used solutions. The slope of the linear fit obtained from all points plus the Cartesian (0,0) gave the desired value. Figure S1 shows the absorption spectra of the compounds in toluene, and the plot of absorbance vs. molar concentration for FM**,** with its linear fit for subsequent molar decadic coefficient calculation.

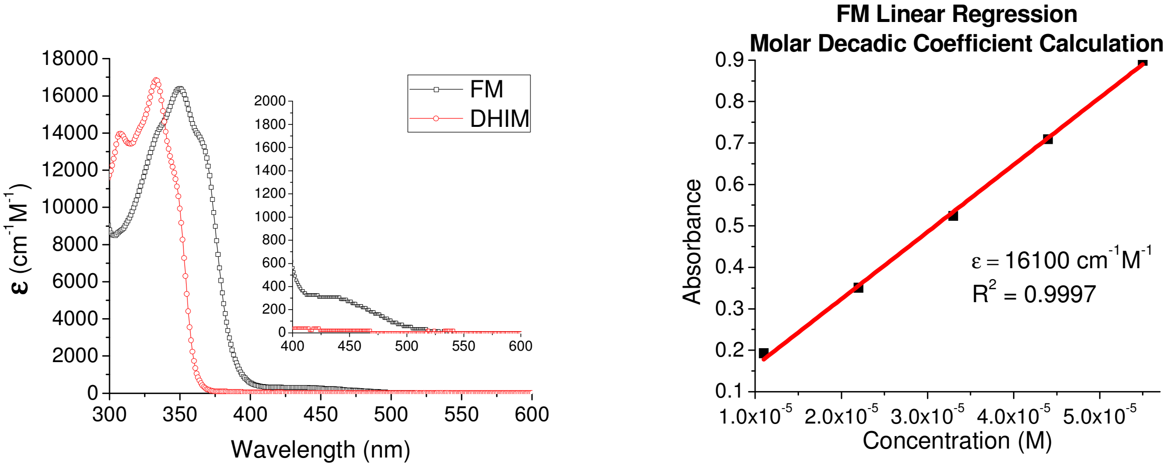

Figure S1. Molar absorptivity calculation – *Left*: Absorption spectra of final compounds in toluene. *Right*: Plot of Absorbance vs. Molar Concentration for FM in toluene at 350 nm.

The absorption characteristics of all compounds were measured with solvents of different polarities (toluene, THF, DMF). Figure S2 shows the absorption spectra of the final compounds in the aforementioned solvents. See that there is a negligible solvent dependence of the vertical absorptions in both compounds.

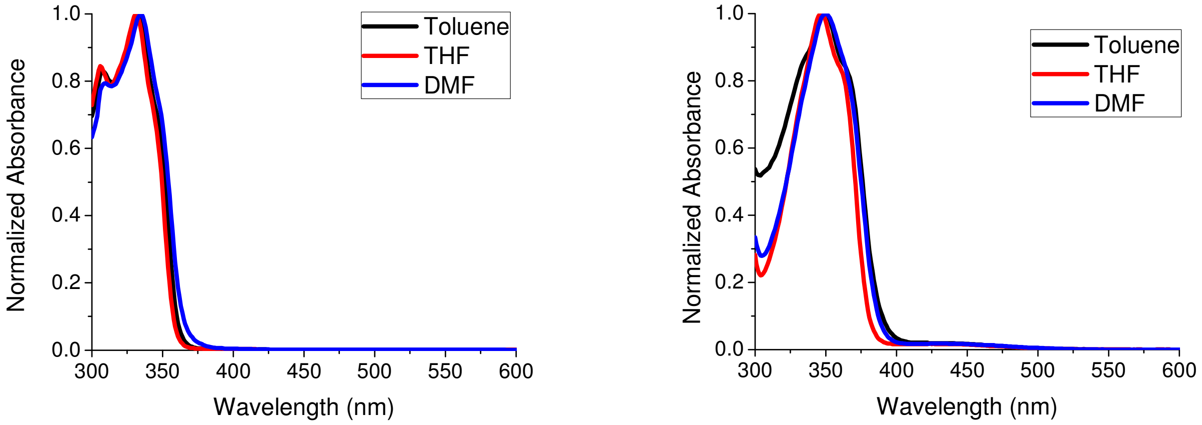

Figure S2. Absorption spectra of IM (left) and FM (right) in toluene, THF and DMF.

4. Emission Measurements.

Steady-state fluorescence measurements were performed on a single-photon-counting spectrofluorimeter equipped with pulsed NanoLEDs for emission lifetime measurements. Solutions with optical densities below 0.1 at the wavelength of excitation were prepared in the following spectroscopic grade toluene. For fluorescence studies at 77 K, the compounds were dissolved in spectroscopic grade 2-methyltetrahydrofuran (MeTHF), modulating their concentrations until their optical densities were ranging between 0.1 and 0.3. A transparent quartz dewar containing liquid N_2 was used to form the glasses (*in situ*). No signal was found for each of the studied compounds neither at room temperature nor at 77 K, thus suggesting that the relaxation path after photoexcitation is exclusively non-radiative.

5. Time resolved UV-Vis picosecond transient absorption measurements.

The picosecond time-resolved apparatus at the Ohio Laboratory for Kinetic Spectrometry at Bowling Green State University has been described elsewhere.[5] In short, the laser source generated pulses of 1mJ, 100 fs (fwhm), 800 nm light operating at a repetition rate of 1.00 kHz. The mother beam is split into pump (85%) and probe (15%) beams. The former beam was converted into the selected excitation wavelength by means of an Optical Parametric Amplifier (OPA), and attenuated through a half-wave plate to make sure that its intensity was <3μJ when in contact with the sample. The latter beam was passed through a delay stage which provided a resolution of ~7 fs steps into a 1600 ps time frame. The pump beam was passed through an optical chopper (operating frequency=100 Hz) and focused into the 2 mm path length sample cell where it was overlapped with the probe white light continuum beam generated by a CaF_2 plate (effective useful range: 340–790 nm) after the delay stage, at an angle of ca. 5°. The probe light was coupled into a 400 μm optical fiber connected to a CCD spectrograph. The delay line and the CCD spectrograph were computer-controlled by a software routine developed in-house. The sample was dissolved in spectroscopic grade toluene or DMF and transferred to a quartz cell with an optical path of 2 mm. Steady state UV-Vis absorption measurments were carried out before and after laser irradiate to monitor any sample decomposition. All measurements were carried out at room temperature (20 ± 2 C°). Signal decay/rise data analysis was carried out by using (mathematical method) deconvolution of single exponential models. Figure S3 shows the global fits for the ΔOD of the absorption bands centered at 405 and 600 nm, whereby such absorptions displayed the same kinetics accounting for the deactivation of the same singlet state.

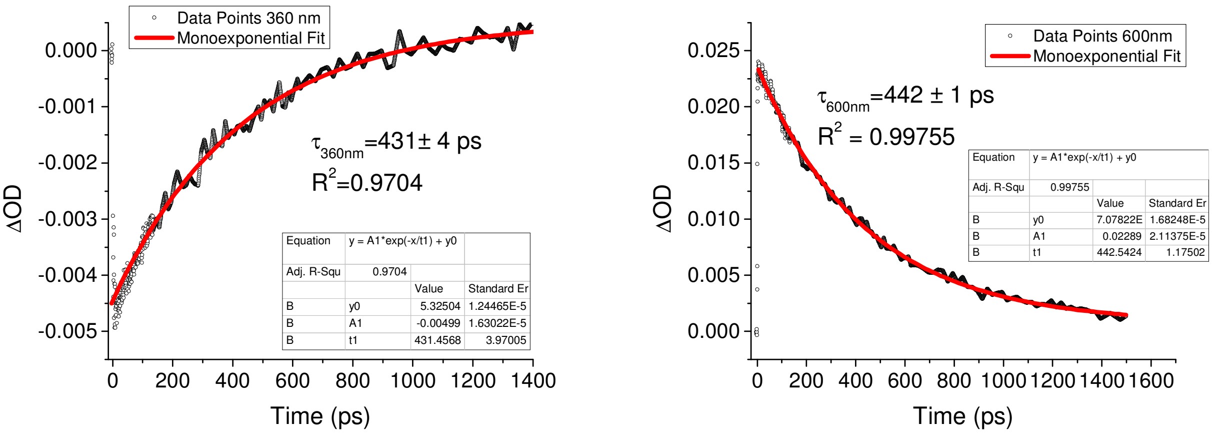

Equation	y = A1*exp(-x/t1) + y0		
Adj. R-Squ	0.9704		
		Value	Standard Er
B	y0	5.32504	1.24465E-5
B	A1	-0.00499	1.63022E-5
B	t1	431.4568	3.97005

Equation	y = A1*exp(-x/t1) + y0		
Adj. R-Squ	0.99755		
		Value	Standard Er
B	y0	7.07822E	1.68248E-5
B	A1	0.02289	2.11375E-5
B	t1	442.5424	1.17502

Figure S3. Kinetic traces at 360 nm (left) and 600 nm (right).

6. Computational Procedures.

Vertical absorption energies

The ground state geometries were optimised with the complete-active-space self-consistent field (CASSCF) method, demanding one root in the CASSCF procedure and including only the π out-of-plane natural orbitals (NOs) in the active space. The ANO-L-VDZP basis set, as a good compromise between accuracy and computational cost, was used both in the optimisations and the vertical absorption studies. The selected active spaces for the single-point calculations on the DCE, IM and FM optimised structures, according to the calibration shown in Tables 2 and 3, are displayed in Figures S4-S7. Five, ten and five roots were demanded in the state-average (SA)-CASSCF method for the DCE, IM and FM compounds, respectively. The complete-active-space second-order perturbtion theory (CASPT2)[6] method was used to include the dynamical electron correlation, maintaining the core electrons frozen in the perturbation step. In order to minimise the effect of weakly interacting intruder states, the imaginary level-shift technique, with the recommended value of 0.2 au, was employed throughout.[7] The CASPT2 method with the zeroth-order Hamiltonian as originally implemented (ionisation potential electron affinity parameter set to 0.0 au) was used. All the calculations were performed with the MOLCAS 8 software package.[8]

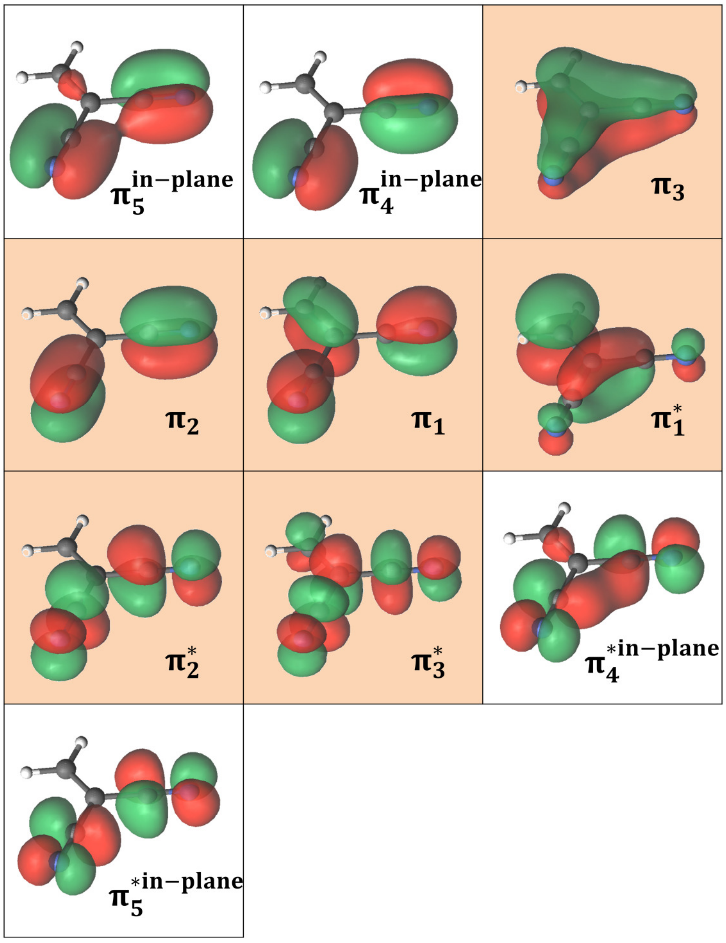

Figure S4. Optimised structure and NOs included in the (10,10) active space for the DCE model. Orbitals in shady boxes compose the (6,6) active space (see main text).

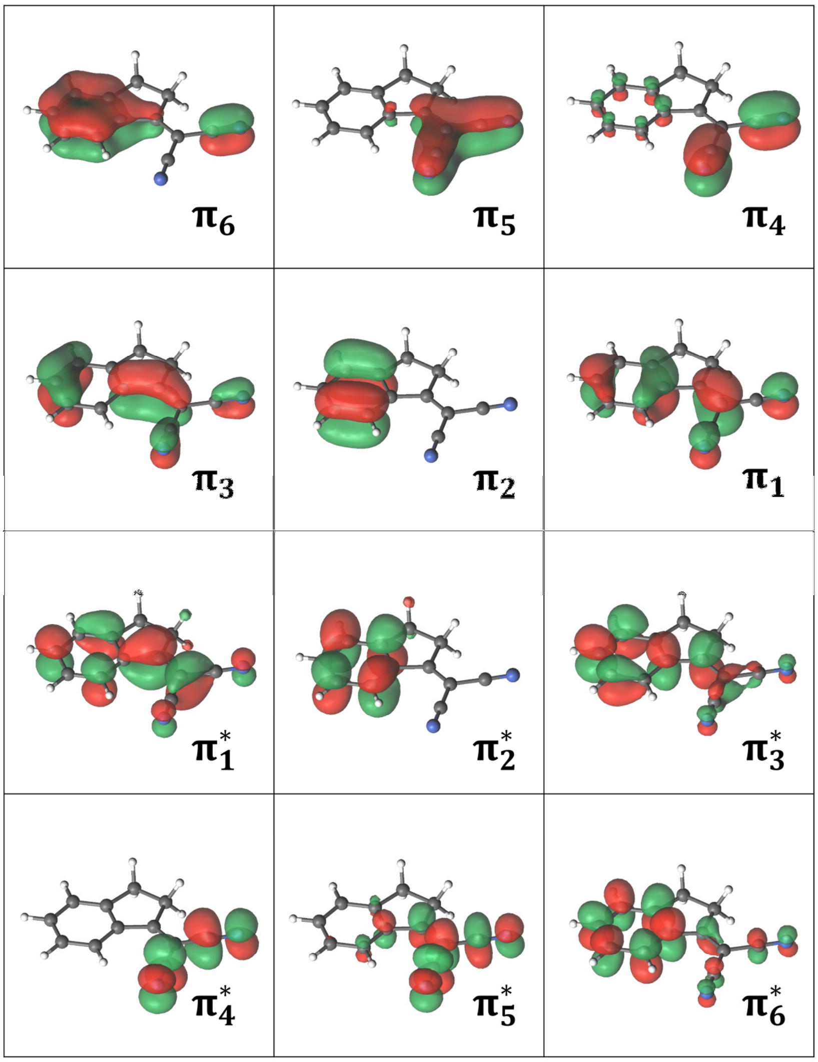

Figure S5. Optimised structure and NOs included in the active space $(12,12)_{\text{out}}$ of IM.

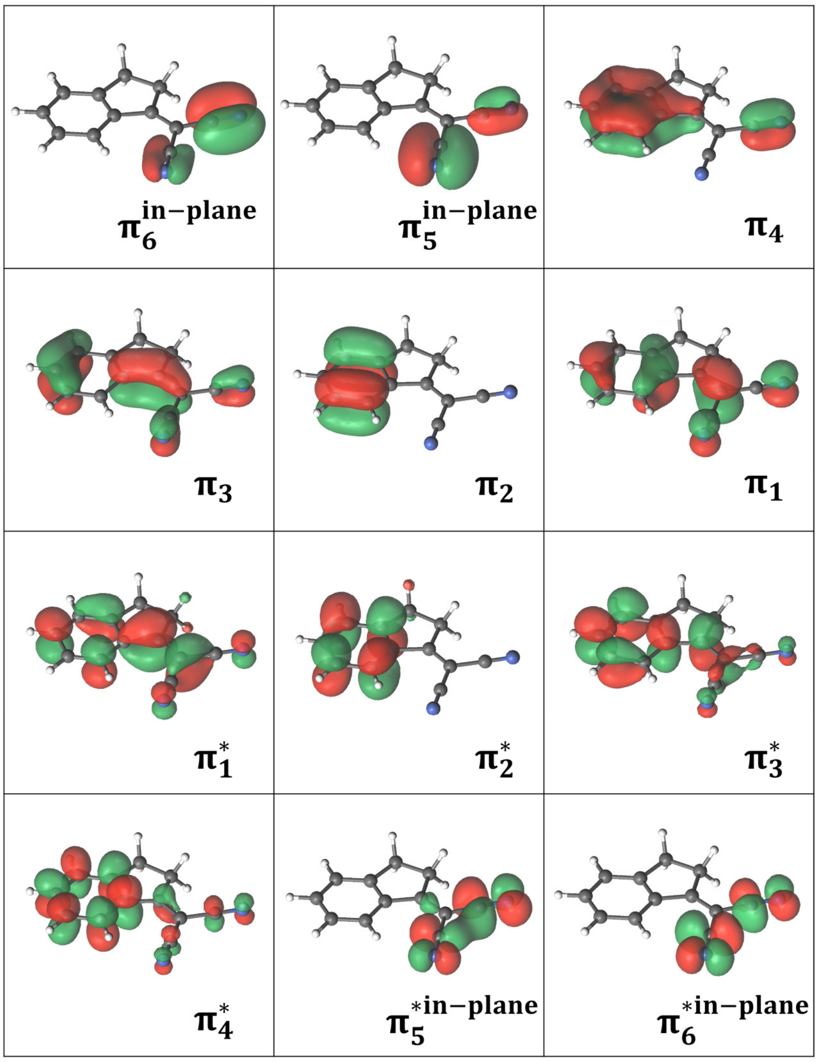

Figure S6. Optimised structure and NOs included in the active space $(12,12)_{in}$ of IM.

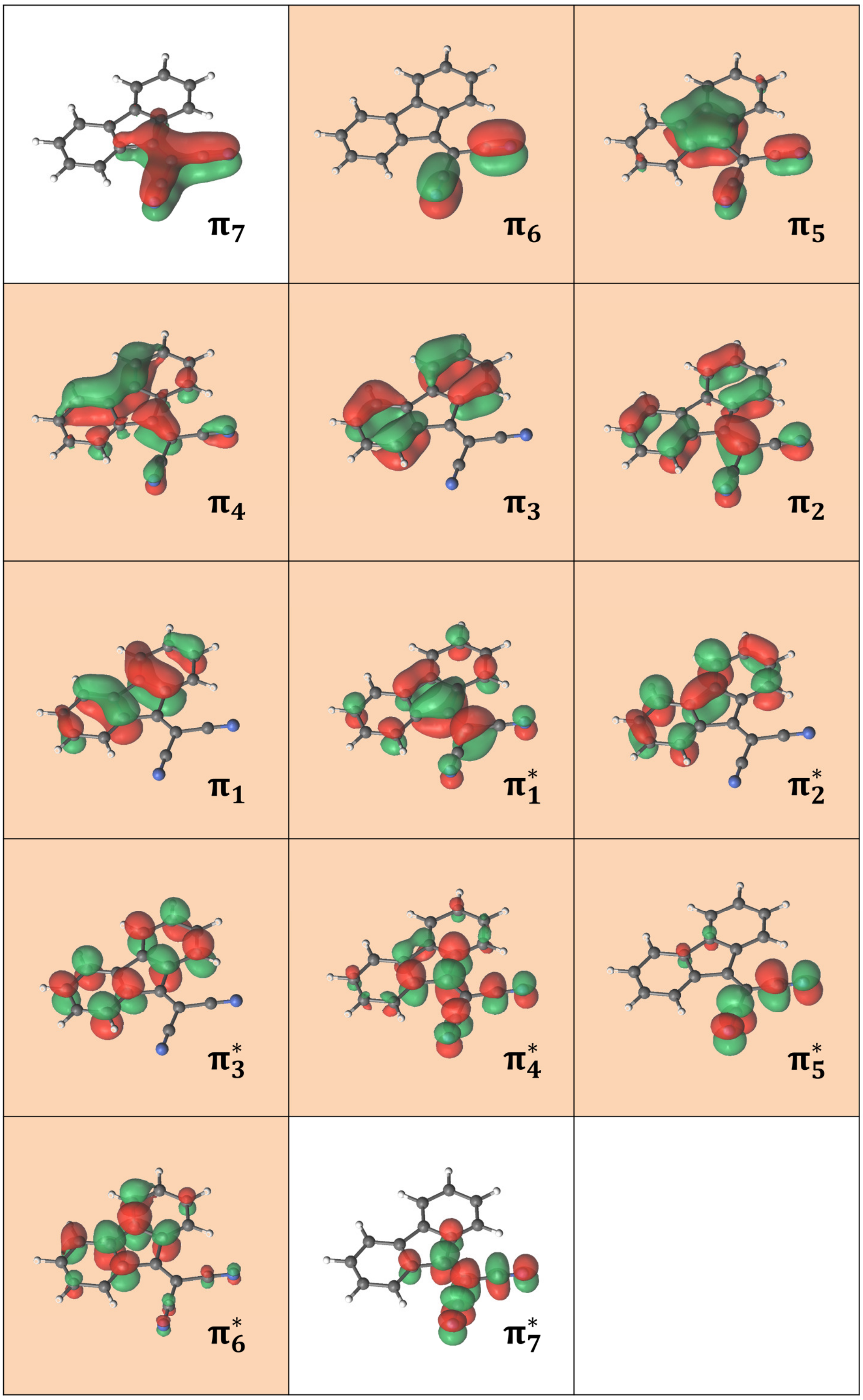

Figure S7. Optimised structure and NOs included in the active space (14,14) of FM. Orbitals in shady boxes compose the (12,12) active space (see main text).

Calibration of the CASPT2//CASSCF/ANO methodological approach

Basis set

The converngence of the results on the size of the basis set was calibrated in the IM system. In order to do that, the absorption energies were evaluated considering the double-ζ ANO-S-VDZP, ANO-L-VDZP and triple-ζ ANO-L-VTZP basis sets. The $(12,12)_{out}$ active space (see Fig. S5) was used for the calibration, demanding five roots in the SA-CASSCF procedure. Results are summarised in Table S1. Energy differences lower than 0.1 eV were computed with the ANO-S-VDZP and ANO-L-VDZP basis sets with respect to the ANO-L-VTZP reference values. According to these results, the ANO-L-VDZP basis set was used for the computation of the vertical absorption energies whereas the cheaper ANO-S-VDZP basis set was used for the calculation of the decay pathways.

Table S1. CASPT2 vertical absorption energies (eV) of IM using different ANO-type basis sets.

State	ANO-S-VDZP	ANO-L-VDZP	ANO-L-VTZP
S_1	4.07	4.00	3.99
S_2	4.26	4.27	4.14
S_3	5.47	5.26	5.36
S_4	5.75	5.65	5.64

CASSCF geometries

In order to check the reliability of the geometries obtained with the CASSCF method, the IM system was optimised using the DFT/M06-2X/6-31++G(d,p) method as implemented in the GAUSSIAN 09 suite of programs.[9] Thereby, on top of the converged geometry, the vertical absorption energies for the low-lying states were computed with the CASSCF/CASPT2 method. CASPT2 excited-state energies at both CASSCF and DFT/M06-2X geometries are compared in Table S2. Negligible differences are found between both computational strategies, validating thus the CASSCF geometries.

Table S2. CASPT2 vertical absorption energies (eV) of the IM system computed at the CASSCF and M06-2X optimised geometries.

State	CASSCF/ANO-L-VDZP	M06-2X/6-31++G(d,p)
S_1	4.00	3.98
S_2	4.27	4.18
S_3	5.26	5.22
S_4	5.65	5.64

Number of roots for the SA-CASSCF/CASPT2 single-point calculations

The number of states computed in the SA-CASSCF procedure can have a significant impact on the excited-state energies computed at the CASPT2 level. In order to evaluate such impact and consequently determine the best number of roots for the calculations on the present compounds, a systematic study increasing progressively the number of roots has been performed on the DCE, IM and FM compounds. Results are compiled in Tables S3, S4 and S5. In the case of DCE (Table S3), it can be concluded that at least three roots are required to have a good description of the S_1 state. Furthermore, increasing the number of roots to more than three does not affect significantly the energies of the excited states. Taking into account these findings, five roots were used in the determination of the vertical absorption energies of DCE (Table 2) and three were computed in the study of the decay mechanism. On the other hand, results on the IM system (Table S4) indicate that at least five roots are needed for a proper description of the S_2 and S_3 states. Increasing the number of roots to ten or fifteen does not significantly change the energies of the excited states. According to these results, ten roots were selected as an adequate number of roots for the interpretation of the UV-Vis absorption spectra (Table 3), whereas only five were computed in the calculation of the decay path. Finally, according to the results for FM summarized in Table S5, it is also expected that five roots will provide a good description of the low-lying electronic states of this more computationally expensive compound (Table 4).

Table S3. CASPT2 vertical absorption energies (eV) of DCE using different number of roots in the SA-CASSCF procedure. The ANO-L-VDZP and the (6,6) active space were used throughout.

State	**2**	**3**	**4**	**5**	**10**
S_1	6.95	6.58	6.48	6.49	6.46
S_2		6.95	6.95	6.99	6.96
S_3			7.32	7.29	7.30
S_4				7.46	7.54
S_5					9.48

Table S4. CASPT2 vertical absorption energies (eV) of IM using different number of roots in the SA-CASSCF procedure. The ANO-L-VDZP and the $(12,12)_{out}$ active space were used throughout.

State	**3**	**4**	**5**	**10**	**15**
S_1	4.04	4.00	4.00	4.02	4.03
S_2	5.07	4.68	4.27	4.34	4.22
S_3		4.82	5.26	5.13	5.25
S_4			5.65	5.74	5.79
S_5				5.90	5.82

Table S5. CASPT2 vertical absorption energies (eV) of FM using different number of roots in the SA-CASSCF procedure. The ANO-L-VDZP and the (12,12) and (14,14) active spaces were used in the calculations.

	CASPT2(14,14)		**CASPT2(12,12)**	
State	**3**	**5**	**5**	**10**
S_1	2.83	2.90	2.70	2.62
S_2	3.45	3.50	3.28	3.34
S_3		3.53	3.44	3.38
S_4		4.22	4.01	3.90
S_5				4.39

Solvent effects

Since all the electronic calculations were perfomed *in vacuo* and the experiments carried out in solution, solvent effects were computed for the absorption energies in order to have an estimation of changes due to solvation. To do that, the IM compound was optimised using the DFT method (CAM-B3LYP and M06-2X functionals) with and without the polarizable continuum model (PCM) method,[10] as implemented in GAUSSIAN 09 software package.[9] The time-dependent (TD)-DFT and TD-DFT-PCM methods were subsequently employed for the calculation of the ground and the first four low-lying excited states, on top of the corresponding DFT or DFT-PCM optimised structures. Results are summarised in Table S6. It can be readily seen that the stabilisation due to the solvent is smaller than 0.2 eV in all the states, where the S_1 and the S_2 states have the largest changes. Additionally, the solvent estimation does not change the ordering of the states, providing the same qualitative description using both TD-DFT and TD-DFT-PCM approaches. It can be therefore concluded that, according to the small solvent effects predicted for the studied systems, the *in vacuo* theoretical methods used in this work are capable of interpret the experimental signals measured in solution.

Table S6. Vertical excitation energies (eV) computed using the TD-DFT and the TD-DFT-PCM methods at the geometries optimised with the DFT and DFT-PCM methods, respectively, for the IM system.

State	**TD-CAM-B3LYP/6-31++G(d,p)**		**TD-M06-2X/6-31++G(d,p)**	
	In vacuo	*PCM*	*In vacuo*	*PCM*
S_1	4.27	4.10	4.31	4.13
S_2	4.66	4.57	4.71	4.62
S_3	5.94	5.83	5.76	5.68
S_4	5.97	5.89	5.95	5.94

CASPT2 Ionisation-potential electron-affinity parameter

The ionisation-potential electron-affinity (IPEA) parameter[11] of the CASPT2 method has been also calibrated on the IM system, using the ANO-L-VDZP basis set, the $(12,12)_{out}$ active space (see Figure S5) and demanding five roots in the SA-CASSCF procedure. Results are summarised in Table S7. As compared with the experimental band maximum (see Figure 2), the best agreement is obtained the original zeroth-order Hamiltonian (IPEA = 0.0 au). Higher IPEA values systematically increases the absorption energies.

Table S7. CASPT2 vertical absorption energies (eV) using different values of the IPEA parameter (au) for the IM system.

State	**0.0**	**0.1**	**0.2**	**0.3**	**Exp.**
S_1	4.00	4.21	4.35	4.49	
S_2	4.27	4.46	4.61	4.74	3.74
S_3	5.26	5.48	5.63	5.76	
S_4	5.65	5.96	6.18	6.37	

Multistate CASPT2 calculations

The vertical absorption energies of both IM and FM compounds were also computed with the multistate (MS)-CASPT2 method. Results are compiled in Table S8. For the IM system, it can be readily seen that the MS-CASPT2 method provides a good agreement between the theoretical absorption energy predicted for S_2 (3.85 eV) and the experimental band maximum recorded at ~3.8 eV (see Figure 2). On the contrary, for the FM compound the theoretical method underestimates the energy of the S_2 state in about ~0.4 eV, compared to the experimental band maximum measured at ~3.5 eV. Taking into account that the computed values are in vaccuo and the computed solvent effects decreases the absorption energies, the MS-CASPT2 results deviates in general from the experimental data. In addition, to avoid unphysical results in the S_0/S_1 degeneracy areas, which might arise in the MS-CASPT2 computations, the conventional single-state CASPT2 method was chosen in the present study. This choice is motivated by the fact that the effective Hamiltonian matrix has asymmetric elements with differences up to close to 0.2 eV at the Franck-Condon region.

Table S8. MS-CASPT2 vertical absorption energies (eV), experimental band maxima (eV) and *f* (in brackets) for the IM and the FM compounds.

State	**IM**		**FM**	
	MS-CASPT2	*Exp.*	*MS-CASPT2*	*Exp.*
S_1	3.43 (0.2629)		2.89 (0.0050)	
S_2	3.85 (0.4860)	~3.8	3.14 (0.3964)	~3.5
S_3	5.03 (0.1103)		3.62 (0.0833)	
S_4	5.46 (0.0033)		4.77 (0.0482)	

RASSCF/RASPT2 calculations

The restricted-active-space self-consistent field (RASSCF) method[1213] was used to build multiconfigurational wave functions including all the valence orbitals in the active space, allowing a maximum of two holes in the RAS1 subspace and a maximum of two electrons in the RAS3 subspace. For the IM system, the distribution scheme of the 16 valence NOs within the RAS1, RAS2 and RAS3 subspaces was as follows: 2 $\pi_{CN}^{in-plane}$ plus 3 π NOs in the RAS1 subspace, 3 π plus 3 π* NOs in the RAS2 subspace and 3 π* plus 2 $\pi_{CN}^{*\,in-plane}$ NOs in the RAS3 subspace. On the other hand, the 22 valence NOs of the FM system were distributed in a similar manner: 2 $\pi_{CN}^{in-plane}$ plus 6 π NOs in the RAS1 subspace, 3 π plus 3 π* NOs in the RAS2 subspace and 6 π* plus 2 $\pi_{CN}^{*\,in-plane}$ NOs in the RAS3 subspace.The electronic energies were corrected using the restricted-active-space second-order perturbation theory (RASPT2) method[14,15] and compared with the CASPT2 results. RASPT2 vertical absorption energies are summarised in Table S9. As discussed in the subsection 2.3.1, the $\pi_{CN}^{in-plane}$ and $\pi_{CN}^{*\,in-plane}$ NOs do not participate in the absorption processes and moving them out of the active space do not change significantly the energies of the low-lying electronic states. This finding validates therefore the commputations with the reduced active spaces in which that NOs are excluded. Moreover, the good agreement of energies between both CASPT2 and RASPT2 methods supports the use of the CASPT2 method for the calculation of the decay mechanisms of the lowest-energy excited states.

Table S9. RASPT2 and CASPT2 vertical absorption energies (eV) and *f* (in brackets) for the IM and the FM compounds.

State	**IM**		**FM**	
	CASPT2(12,12)$_{out}$	*RASPT2*	*CASPT2(14,14)*	*RASPT2*
S$_1$	4.02 (0.0213)	4.12 (0.0334)	2.90 (0.0002)	2.82 (0.0006)
S$_2$	4.34 (0.5106)	4.25 (0.6123)	3.50 (0.0613)	3.65 (0.0287)
S$_3$	5.13 (0.1814)	5.44 (0.0232)	3.53 (0.1761)	3.71 (0.2712)
S$_4$	5.74 (0.0675)	5.53 (0.0675)	4.22 (0.2962)	4.65 (0.1162)

Photochemical decay channels

Minimum energy path (MEP) calculations on the DCE system

Minimum energy path (MEP) computations were carried out using the ANO-S-VDZP basis set and the CASSCF method and an active space comprising all the in-plane and out-of-plane π and π* orbitals, that is, the (10,10) active space, as displayed in Figure S4. MEPs were built as steepest descendent paths, as explained elsewhere.[16] The radius of the hypersphere was set to 0.1 au. Mass-weighted coordinates were used. On top of the converged MEP points, the CASSCF/CASPT2/ANO-S-VDZP calculations were perfomed using the (10,10) and also the (6,6) active space. Three roots were averaged in the CASSCF procedure. Figure 6 displays the MEP results using the (10,10) active space both for the optimisations and the CASPT2 single-point calculations, *i.e.* CASPT2(10,10)//CASSCF(10,10). The results using the (6,6) active space on top of the geometries minimised employing the (10,10) active space are displayed in Figure S8.

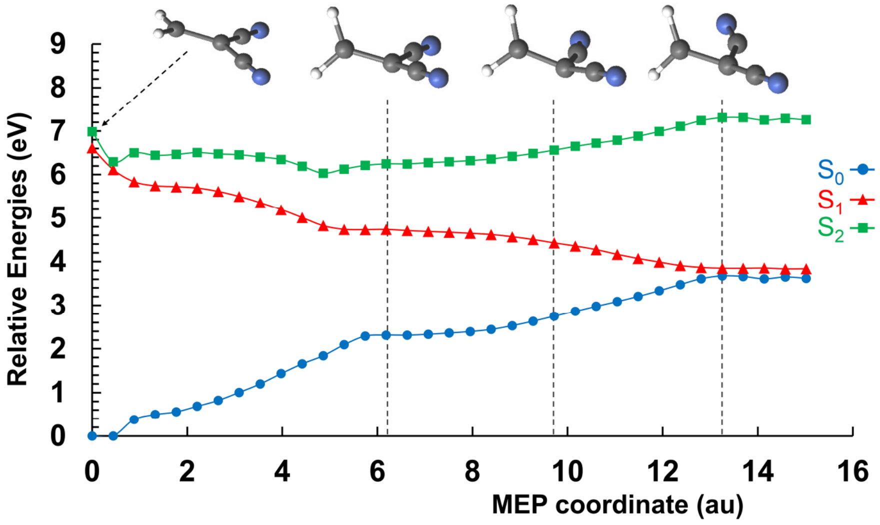

Figure S8. CASPT2(6,6)/ANO-S-VDZP energies of the S0 and S1 states of the DCE system computed at the CASSCF(6,6)/ANO-S-VDZP MEP optimised geometries.

Pyramidalisation studies on the DCE, IM and FM systems

The CASSCF method and the C_s symmetry constraint were used for geometry optimisations. The equilibrium structures of the lowest states of symmetry A' of the planar and twisted molecules were optimised. The double-ζ basis set of atomic natural orbital type ANO-S-VDZP was used throughout. All the valence out-of-plane π and π^* orbitals were employed in the CAS space for the DCE and IM computations. It corresponds to the (6,6) and $(12,12)_{out}$ active spaces, respectively. For FM, the (12,12) active space was used. In order to characterise the PESs of the ground state and the lowest-lying excited states along the coupled motion of torsion and pyramidalisation (Figs. 6, 8 and 9), the energies of the S_0-S_2 states for DCE and the S_0-S_4 states for IM and FM were calculated with the CASPT2 method without symmetry constraints and the following strategy was employed. First, 10 geometries (points 2-11 in the figures) were generated by linearly interpolating the internal coordinates of the CASSCF optimised planar (point 1) and twisted (point 12) structures. The other structures (points 13-18, for DCE and IM, and points 13-23, for FM) corresponds to different values of the pyramidalisation angle keeping the remaining degrees of freedom fixed to those of the optimised twisted geometry. In particular, 6 pyramidalisation angles were mapped from the optimised values (131° and 160° for DCE and IM, respectively) in the range 122-72° and 131-81° for DCE and IM, respectively, in steps of 10°. For FM, the pyramidalisation angles were mapped from the optimised value of 180° in the range 170-70° and also in steps of 10°. The energy profile of the DCE was also computed at a higher level of theory using the (10,10) active space and five averaged roots in the SA-CASSCF procedure. The results obtained (see Fig. S9) show no significant differences with respect to the findings obtained at the CASPT2(6,6) level and averaging 3 roots in the SA-CASSCF. Regarding the study of the pyramidalisation of IM in the *syn* and *anti* directions, in Fig. 9, the lowest-energy state of symmetry A' and A'' were computed with the CASPT2 method. The pyramidalisation distortion was mapped around the optimised values for the *anti* and *syn* directions (154° and 160°, respectively) at the angles 81, 91, 101, 111, 121, 131 and 179°.

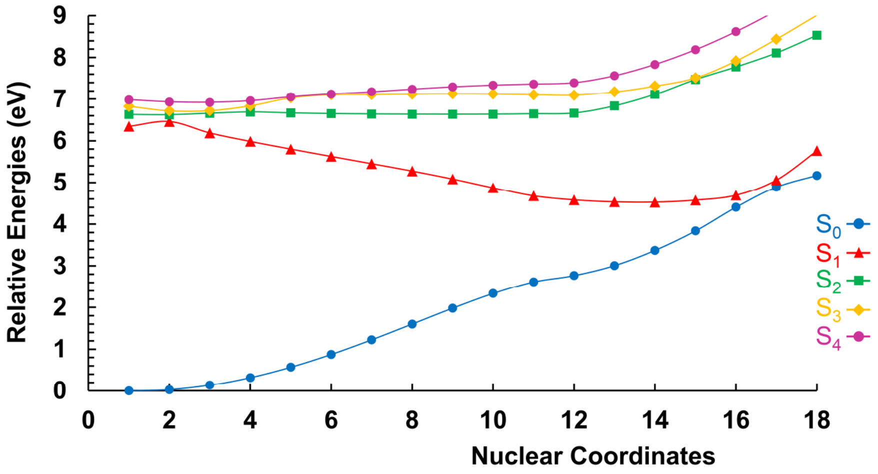

Figure S9. Adiabatic CASPT2//CASSCF(10,10)/ANO-S-VDZP potential energy surfaces of the S_0, S_1 and S_2 states of the model compound DCE mapped along the coupled torsion and pyramidalisation coordinates.

Role of triplet states

Table S10. CASPT2 vertical energies (E_T, in eV) of the ten lowest-lying triplet states of IM at the S_0 minimum geometry. The $(12,12)_{in}$ active space and the ANO-L-VDZP basis set have been used in the computations. MO labelling is displayed in Figure S6.

State	E_T	Nature of the main one-electron transition(s)
T$_1$	2.73	$\pi_1 \rightarrow \pi_1^*$
T$_2$	3.75	$\pi_2 \rightarrow \pi_2^*$ $\pi_3 \rightarrow \pi_1^*$
T$_3$	3.85	$\pi_1 \rightarrow \pi_2^*$ $\pi_2 \rightarrow \pi_1^*$
T$_4$	4.23	$\pi_1 \rightarrow \pi_1^*$ $\pi_1 \rightarrow \pi_2^*$ $\pi_2 \rightarrow \pi_1^*$
T$_5$	4.78	$\pi_1 \rightarrow \pi_2^*$ $\pi_2 \rightarrow \pi_1^*$
T$_6$	5.56	$\pi_2 \rightarrow \pi_3^*$ $\pi_3 \rightarrow \pi_2^*$ $\pi_4 \rightarrow \pi_2^*$
T$_7$	6.15	$\pi_3 \rightarrow \pi_3^*$ $\pi_4 \rightarrow \pi_1^*$
T$_8$	6.64	$\pi_5^{in-plane} \rightarrow \pi_5^{*\,in-plane}$ $\pi_6^{in-plane} \rightarrow \pi_6^{*\,in-plane}$
T$_9$	6.78	$\pi_6^{in-plane} \rightarrow \pi_6^{*\,in-plane}$ $\pi_5^{in-plane} \rightarrow \pi_5^{*\,in-plane}$
T$_{10}$	7.02	*double excitations*

7. Notes and references

1 L. A. Estrada and D. C. Neckers. *J. Org. Chem.* 2009, **74**, 8484.

2 D. Xue, Y.-C. Chen, X. Cui, Q.-W. Wang, J. Zhu and J.-G. Deng. *J. Org. Chem.* 2005, **70**, 3584.

3 W.-Y. Wong, G.-L. Lu, K.-H. Choi, Z. Lin, Eur. J. Org. Chem. 2003, 365; A. Sliwinska, W. Czardybon and J. Warkentin. *Org. Lett.* 2007, **9**, 695.

4 From both references in 3, only that of Warketin et al. reports the ^{13}CNMR of the compound where only 7 peaks are assigned. Considering that FM has C2v symmetry, the number of chemically non-equivalent carbons total 9. We believe that the mismatch with our spectrum is due to the lack of assignation of two important signals at 75 and 162 ppm which account for the alpha and methylene carbon respectively. The rest of the carbons reported matched satisfactorily with our spectra.

5 A. V. Nikolaitchik, O. Korth and M. A. J. Rodgers *J. Phys. Chem. A* **1999**, *103*, 7587. (b) A. P. Pellicciolli, K. Henbest, G. Kwag; T. R. Carvagno, M. E. Kenney and M. A. J. Rodgers *J. Phys. Chem. A* **2001**, *105*, 1757. (c) A. N. Okhrimenko, A. V. Gusev and M. A. J. Rodgers *J. Phys. Chem. A* **2005**, *109*, 7653.

6 (a) B. O. Roos *Adv. Chem. Phys.* 1987, **67**, 399. (b) K. Andersson, P.-Å. Malmqvist, B. O. Roos *J. Chem. Phys.* 1992, **96**, 1218. (c) D. Roca-Sanjuán, F. Aquilante, R. Lindh *WIREs Comput. Mol. Sci.* 2012, **2**, 585.

7 N. Forsberg and P.-Å. Malmqvist, *Chem. Phys. Lett.* 1997, **274**, 196.

8 F. Aquilante, J. Autschbach, R. K. Carlson, L. F. Chibotaru, M. G. Delcey, L. De Vico, I. Fdez. Galván, N. Ferré, L. M. Frutos, L. Gagliardi, M. Garavelli, A. Giussani, C. E. Hoyer, G. Li Manni, H. Lischka, D. Ma, P. Å. Malmqvist, T. Müller, A. Nenov, M. Olivucci, T. B. Pedersen, D. Peng, F. Plasser, B. Pritchard, M. Reiher, I. Rivalta, I. Schapiro, J. Segarra-Martí, M. Stenrup, D. G. Truhlar, L. Ungur, A. Valentini, S. Vancoillie, V. Veryazov, V. P. Vysotskiy, O. Weingart, F. Zapata and R. Lindh, *J. Comp. Chem.* 2015, **37**, 506.

9 Gaussian 09, Revision C.01, M. J. Frisch, G. W. Trucks, H. B. Schlegel, G. E. Scuseria, M. A. Robb, J. R. Cheeseman, G. Scalmani, V. Barone, B. Mennucci, G. A. Petersson, H. Nakatsuji, M. Caricato, X. Li, H. P. Hratchian, A. F. Izmaylov, J. Bloino, G. Zheng, J. L. Sonnenberg, M. Hada, M. Ehara, K. Toyota, R. Fukuda, J. Hasegawa, M. Ishida, T. Nakajima, Y. Honda, O. Kitao, H. Nakai, T. Vreven, J. A. Montgomery, Jr., J. E. Peralta, F. Ogliaro, M. Bearpark, J. J. Heyd, E. Brothers, K. N. Kudin, V. N. Staroverov, T. Keith, R. Kobayashi, J. Normand, K. Raghavachari, A. Rendell, J. C. Burant, S. S. Iyengar, J. Tomasi, M. Cossi, N. Rega, J. M. Millam, M. Klene, J. E. Knox, J. B. Cross, V. Bakken, C. Adamo, J. Jaramillo, R. Gomperts, R. E. Stratmann, O. Yazyev, A. J. Austin, R. Cammi, C. Pomelli, J. W. Ochterski, R. L. Martin, K. Morokuma, V. G. Zakrzewski, G. A. Voth, P. Salvador, J. J. Dannenberg, S. Dapprich, A. D. Daniels, O. Farkas, J. B. Foresman, J. V. Ortiz, J. Cioslowski and D. J. Fox, Gaussian, Inc., Wallingford CT, 2010.

10 J. Tomasi, B. Menucci and R. Cammi, *Chem. Rev.* 2005, **105**, 2999-3094. (b) M. Cossi, N. Rega, G. Scalmani and V. Barone, *J. Comput. Chem.* 2003, **24**, 669-681.

11 N. Forsberg and P.-Å. Malmqvist, *Chem. Phys. Lett.* 1997, **274**, 196.

12 J. Olsen, B. O. Roos, P. Jorgensen and H. J. A. Jensen, *J. Chem. Phys.* 1988, **89**, 2185.

13 P.-Å. Malmqvist, A. Rendell and B. O. Roos, *J. Phys. Chem.* 1990, **94**, 5477.

14 P.-Å. Malmqvist, K. Pierloot, A. R. M. Shahi, C. J. Cramer and L. Gagliardi, *J. Chem. Phys.* 2008, **128**, 204109.

15 V. Sauri, L. Serrano-Andres, A. R. M. Shahi, L. Gagliardi, S. Vancoillie and K. Pierloot, *J. Chem. Theor. Comput.* 2011, **7**, 153-168.

16 (a) L. De Vico, M. Olivucci and R. Lindh, *J. Chem. Theor. Comput.* 2005, **1**, 1029-1037. (b) I. Schapiro, D. Roca-Sanjuán, R. Lindh and M. Olivucci, *J. Comput. Chem.* 2015, **36**, 312-320.